Multiobjective Dynamic Optimization of an Industrial Nylon 6 Semibatch Reactor Using Genetic Algorithm

K. MITRA,[1] K. DEB,[2] SANTOSH K. GUPTA

[1] Department of Chemical Engineering, Indian Institute of Technology, Kanpur, 208016, India

[2] Department of Mechanical Engineering, IIT, Kanpur 208 016, India

Received 16 May 1997; accepted 3 September 1997

ABSTRACT: The nondominated sorting genetic algorithm (NSGA) is adapted and used to obtain multiobjective Pareto optimal solutions for three grades of nylon 6 being produced in an industrial semibatch reactor. The total reaction time and the concentration of an undesirable cyclic dimer in the product are taken as two individual objectives for minimization, while simultaneously requiring the attainment of design values of the final monomer conversion and for the number-average chain length. Substantial improvements in the operation of the nylon 6 reactor are indicated by this study. The technique used is very general in nature and can be used for multiobjective optimization of other reactors. Good mathematical models accounting for all the physicochemical aspects operative in a reactor (and which have been preferably tested on industrial data) are a prerequisite for such optimization studies. © 1998 John Wiley & Sons, Inc. J Appl Polym Sci 69: 69–87, 1998

Key words: multiobjective optimization, nylon 6, genetic algorithm, polymer reactor, polymerization, Pareto sets

INTRODUCTION

Most real-world decision-making design problems require simultaneous optimization of multiple objectives. Such problems are conceptually different from single-objective optimization problems. In the case of multiobjective optimization, a *set* of solutions is obtained which are not necessarily the best solutions if any of the objectives is considered individually, but are relatively better feasible optimal solutions if all the objectives are considered simultaneously. This set of solutions is called the Pareto optimal or nondominated solutions. In this study, multiobjective optimization of an industrial nylon 6 reactor was carried out and Pareto sets were generated. These help to focus the thinking of a decision maker in identifying suitable operating or design conditions.

A number of studies have been reported on the optimal temperature and initiator or monomer addition histories (or profiles) for free-radical and step-growth polymerizations in batch, semibatch, or plug-flow reactors. These have been reviewed by Farber.[1] In most of the studies discussed in the review, a single-objective function is used which is a weighted average of a few individual objectives as, for example, (a) concentration of the unreacted monomer in the product, (b) concentration of undesirable side products, (c) reaction time, and (d) deviation of the number-average chain length (μ_n) and/or the polydispersity index (PDI) from the desired values. This type of scalar optimization approach suffers from the drawback that the results are highly sensitive to the values

Correspondence to: S. K. Gupta.

Contract grant sponsor: Research Centre, Gujarat State Fertilizers Co. Ltd., Vadodara, India.

Journal of Applied Polymer Science, Vol. 69, 69–87 (1998)

 CCC 0021-8995/98/010069-19

of the weighting factors used. In addition, there is a chance of losing some optimal solutions.[2,3] In vector or multiobjective optimization, the objective function, **I**, is a vector, comprising a few individual objective functions, I_i. The optimal solutions obtained using this approach help a designer to make better decisions. Since most optimization problems in polymer reaction engineering deal with different interesting and often conflicting objectives, multiobjective function optimization offers tremendous prospects for use in the optimal design and operation of these reactors. Some studies[4–9] have already been reported on the optimization of polymerization reactors using this approach, but none of these involves industrial reactors. In this work, we have optimized the operation of an *industrial* nylon 6 reactor. This reactor has been simulated by our group earlier,[10–12] and a satisfactory mathematical model is already available, which can be used confidently for optimization purposes.

Most of the earlier studies on the optimization of polymerization reactors involving single- as well as multiple-objective functions use Pontryagin's minimum principle[13,14] or some pattern search techniques to arrive at optimal solutions. These traditional techniques usually require a good initial guess of the optimal solution, that is, of the control variable histories. It is well known that Pontryagin's technique is particularly sensitive to the choice of the initial guess. In fact, for complex, real-life problems (e.g., for methyl methacrylate polymerization[15] as well as for nylon 6 polymerization[16–18]), the "window" in which the initial guess of the control variable must lie is extremely narrow, and one can easily get into problems of lack of convergence. One often has to generate solutions of similar or easier problems[16,17] before one gets an idea of good initial guesses. These techniques are, thus, not suitable for on-line applications. A new and extremely powerful search technique based on the mechanics of natural genetics and natural selection, called the genetic algorithm (GA),[19] is becoming popular in the literature. This technique does not require initial guesses of the control variable. This is a very robust technique and can be made to converge to the global optimum even in the presence of several local optima. Details of GA as well as of its several adaptations and extensions are available in several books.[19–21] A computer code [simple genetic algorithm) (SGA)] which uses the basic algorithm is available now,[21] and this can be used as such

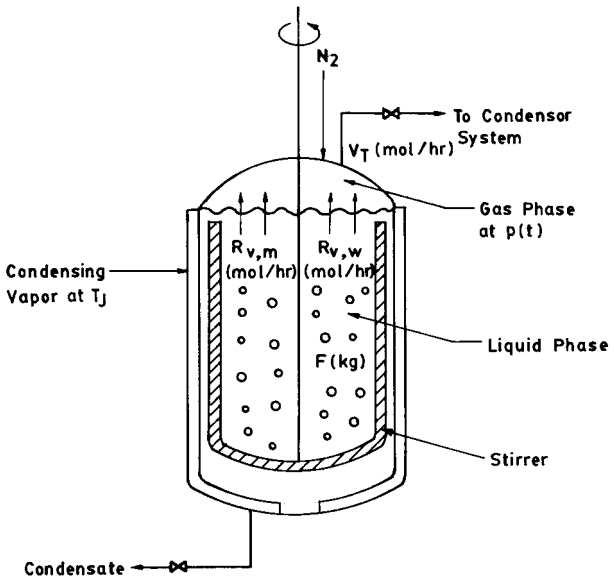

Figure 1 Schematic diagram of the industrial semibatch nylon 6 reactor.

or as a part of any larger code using any adaptation of this algorithm. In this work, however, we used the nondominated sorting genetic algorithm (NSGA[22]) which is quite similar to the SGA except for some differences in the working principle of the selection operator. Details of this adaptation are discussed later.

Pareto sets for the industrial nylon 6 reactor are obtained using this technique. It is found that significant improvements (reduction in reaction time, reduction in the concentration of undesired side product) are indicated by our study, over the current operation of the reactor. We understand that changes in the operating variables have been made in the industrial reactor along the directions suggested by our studies, and considerable improvements have, indeed, been achieved, in terms of the reduction of the reaction time.

FORMULATION

The industrial reactor[10–12] studied herein is shown schematically in Figure 1. It is a jacketed vessel with a low-speed anchor or ribbon agitator used for mixing the highly viscous reaction mass. The reaction mass [ε-caprolactam (C_1), water (W), and other inert additives like TiO_2, etc.] is heated by condensing vapor in a jacket in which the fluid is at temperature T_J (a constant value independent of time). As the polymerization takes

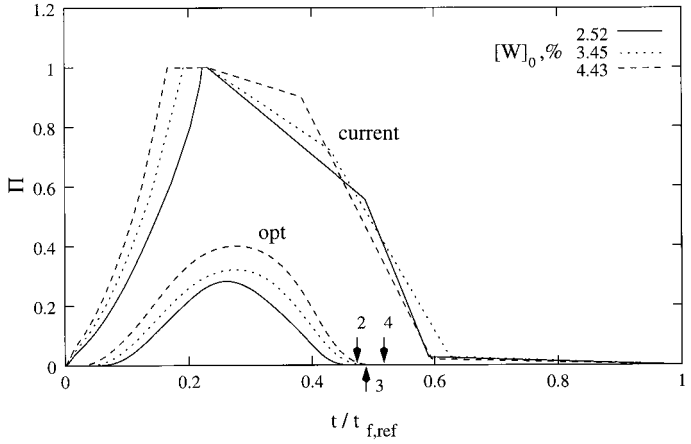

Figure 2 Dimensionless pressure histories used currently to produce three grades of nylon 6, using different values of $[W]_0$.[12] Optimal histories corresponding to points, O_i, in the Pareto optimal solutions also shown. Arrows indicate the values of $t_f/t_{f,\text{ref}}$ for the three $[W]_0$. Values 2, 3, and 4 on the arrows indicate $[W]_0$ = 2.52, 3.45, and 4.43%, respectively.

place, the temperature, T, inside the reactor increases above 220°C and vaporization of ε-caprolactam and water occurs, resulting in a buildup of the pressure, p, in the region above the liquid reaction mass. The pressure inside the reactor, $p(t)$, is maintained such that it conforms to a desired history by manipulation of a control valve. The latter allows the vapor mixture of nitrogen (inert, used initially above the liquid), monomer, and water to pass through to a condenser at a prescribed rate, V_T (mol of mixture/h). The pressure histories used currently for three different industrial runs producing different grades of nylon 6 (using different initial concentrations of water, $[W]_0$), are shown in Figure 2 (curves marked current). In this diagram, the pressure and the time, t, have been nondimensionalized using

$$\prod \equiv (p - p_0)/(p_{\max,\text{ref}} - p_0) \quad \text{(a)}$$

$$\tau \equiv t/t_{f,\text{ref}} \quad \text{(b)} \qquad (1)$$

where $p_{\max,\text{ref}}$ and $t_{f,\text{ref}}$ are the current (indicated by subscript ref) values of the maximum pressure and total reaction time, and p_0 is the initial pressure (see Fig. 2, Current curves). Details of the model used, operating conditions, and results of simulation (for the current or ref conditions), are available in ref. 12 and are not repeated here. Five model parameters were "tuned" using only one set (one value of $[W]_0$) of industrial data, and it was found that this tuned model gave results which compared satisfactorily with industrial data for the other two grades of polymer produced, without requiring any retuning of the model parameters. This indicated that all the physicochemical phenomena playing an important role in the reactor are being correctly modeled. The model[12] is used without any change for multiobjective optimization.

The kinetic scheme for nylon 6 polymerization is given in Table I.[23–25] This scheme incorporates three important reactions, namely, ring opening, polycondensation, and polyaddition, as well as two side reactions involving the cyclic dimer, C_2. Because of the nonavailability of precise information about the rates of reactions involving the higher cyclic oligomers, C_3, C_4, ..., these have not been incorporated in Table I. Since the cyclic dimer constitutes a major share of the total cyclic oligomers in the reaction mass (approximately 25–35 wt %[24, 25], the exact value depending on the operating conditions), this simplification of the kinetic scheme is justified. The "state" of the reactor can be well described by a set of 15 state variables,[12] $\mathbf{x}\{\equiv [x_1, x_2, \ldots, x_{15}]^T\}$. Equations for these can easily be written using mass and energy balances and by obtaining moments of the polymer chain-length distribution are given in ref. 12. In general, the state variable equations can be written in the form

$$\frac{dx_i}{dt} = f_i(\mathbf{x}, \mathbf{u}); \; i = 1, 2, \ldots, 15 \qquad (2)$$

Table I Kinetic Scheme for Nylon 6 Polymerization[23–25] and Corresponding Rate Parameters

1. Ring opening	$C_1 + W \overset{k_1}{\rightleftharpoons} S_1$ $k_1' = \frac{k_1}{K_1}$
2. Polycondensation	$S_n + S_m \overset{k_2}{\rightleftharpoons} S_{m+n} + W;\ n, m = 1,2,\ldots$ $k_2' = \frac{k_2}{K_2}$
3. Polyaddition	$S_n + C_1 \overset{k_3}{\rightleftharpoons} S_{n+1};\ n = 1,2,\ldots$ $k_3' = \frac{k_3}{K_3}$
4. Ring opening of cyclic dimer	$C_2 + W \overset{k_4}{\rightleftharpoons} S_2$ $k_4' = \frac{k_4}{K_4}$
5. Polyaddition of cyclic dimer	$S_n + C_2 \overset{k_5}{\rightleftharpoons} S_{n+2};\ n = 1,2,\ldots$ $k_5' = \frac{k_5}{K_5}$

$$k_i = A_i^0 \exp(-E_i^0/RT) + A_i^c \exp(-E_i^c/RT) \sum_{n=1}^{\infty} ([S_n]) = k_i^0 + k_i^c \sum_{n=1}^{\infty} ([S_n])$$

$$K_i = \exp[(\Delta S_i - \Delta H_i/T)/R],\quad i = 1,2,\ldots,5$$

i	A_i^0 (kg mol^{-1} h^{-1})	E_i^0 (J/mol)	A_i^c (kg^2 mol^{-2} h^{-1}	E_i^c (J/mol)	ΔH_i (J/mol)	ΔS_i (J mol^{-1} K^{-1})
1	5.9874×10^5	8.3198×10^4	4.3075×10^7	7.8703×10^4	$+8.0268 \times 10^3$	-3.2997×10^1
2	1.8942×10^{10}	9.7389×10^4	1.2114×10^{10}	8.6504×10^4	-2.4883×10^4	$+3.9496 \times 10^0$
3	2.8558×10^9	9.5606×10^4	1.6377×10^{10}	8.4148×10^4	-1.6923×10^4	-2.9068×10^1
4	8.5778×10^{11}	1.7577×10^5	2.3307×10^{12}	1.5652×10^5	-4.0176×10^4	-6.0766×10^1
5	2.5701×10^8	8.9141×10^4	3.0110×10^9	8.5374×10^4	-1.3263×10^4	$+2.4384 \times 10^0$

where $\mathbf{x}$ and $\mathbf{u}$ are the vectors of the state and the control variables.

The ordinary differential equations (ODEs) in eq. (2) can be integrated using the D02EJF subroutine of the NAG library for any given $\mathbf{u}(t)$ and initial conditions. This subroutine uses Gear's technique for integrating sets of stiff ODEs.[26] The presence of some discontinuities and the stiffness of the ODEs makes it difficult to use a constant error tolerance (TOL) in the computer code, D02EJF. Provision was made in the algorithm for self-adjustment of the error tolerance between 10^{-12} and 10^{-4}. If the set of ODEs cannot be integrated for a certain value of TOL, the simulation package increases the value of this parameter by a factor of 10 and integrates the set of differential equations again from the previous value of t (for which convergence has been attained). This is attempted between lower and upper limits of TOL. This simulation package is combined with an adaptive version of the NSGA[22] optimization code for performing multiobjective optimization.

Two objective functions (both to be minimized) are considered in this study: The first involves the nondimensional reaction time, $t_f/t_{f,\mathrm{ref}}$. The total reaction time, t_f, is determined as the time at which the monomer conversion, conv, reaches the desired value, $\mathrm{conv}_{f,\mathrm{ref}}$ (the value obtained in in-

dustry presently) as well as the degree of polymerization, $\mu_{n,f}$, reaches the desired value, $\mu_{n,\mathrm{ref}}$. The monomer conversion in a semibatch reactor at any time, t, is defined as

$$\mathrm{conv} \equiv 1 - \frac{F[C_1] + \zeta_1}{F_0[C_1]_0} \tag{3}$$

where F and $[C_1]$ represent the total mass of the liquid reaction mixture and the concentration (mol/kg) of the monomer at any time, respectively, and the subscript 0 represents the initial values. ζ_1 is the (cumulative) amount (mol) of the monomer that has vaporized until time t.

The first of the above requirements (on conv) ensures that the monomer recycling load remains the same as at present, while the second requirement (on μ_n) ensures that the physical properties of the polymer product (determined by μ_n primarily) are the same as those of the polymer currently produced. One may or may not be able to satisfy both of these two requirements at $t = t_f$ simultaneously. To account for this, the integration of the model equations [eq. (2)] is terminated at the point where $\mathrm{conv} = \mathrm{conv}_{f,\mathrm{ref}}$. This denotes the point t_f. The value, $\mu_{n,f}$, of μ_n at this point is incorporated in the first objective function, I_1, in the form of a penalty function with a weightage factor, w_1:

$$I_1 = t_f/t_{f,\mathrm{ref}} + w_1(1 - \mu_{n,f}/\mu_{n,\mathrm{ref}})^2 \tag{4}$$

Minimization of I_1 leads to an increase in the production capacity of the industrial plant (through $t_f/t_{f,\mathrm{ref}}$), while simultaneously giving preference to solutions satisfying the requirement $\mu_{n,f} = \mu_{n,\mathrm{ref}}$ (along with $\mathrm{conv}_f = \mathrm{conv}_{f,\mathrm{ref}}$).

The second objective function, I_2, involves the nondimensional concentration, $[C_2]_f/[C_2]_{f,\mathrm{ref}}$, of the undesirable cyclic dimer in the polymer produced. These cyclics cause problems in polymer processing[23–25] and are removed by hot-water extraction, which is an energy-consuming process. Minimization of $[C_2]_f/[C_2]_{f,\mathrm{ref}}$, thus, leads to the improvement of the product quality, as well as reducing extraction costs downstream. The penalty on the violation of $\mu_{n,f} = \mu_{n,\mathrm{ref}}$ is also included in I_2 with the weightage factor, w_2. Thus,

$$I_2 = [C_2]_f/[C_2]_{f,\mathrm{ref}} + w_2(1 - \mu_{n,f}/\mu_{n,\mathrm{ref}})^2 \tag{5}$$

The use of penalty functions involving $\mu_{n,f}$ in both the objective functions, and the use of the condition, $\mathrm{conv}_f = \mathrm{conv}_{f,\mathrm{ref}}$, to stop the integration of the state variable equations, ensures that we obtain optimal solutions where $t_f/t_{f,\mathrm{ref}}$ and $[C_2]_f/[C_2]_{f,\mathrm{ref}}$ are minimized, while ensuring that $\mathrm{conv}_f = \mathrm{conv}_{f,\mathrm{ref}}$ as well as $\mu_{n,f} = \mu_{n,\mathrm{ref}}$.

The two objectives [eqs. (4) and (5)] are conflicting in nature and, therefore, provide an excellent opportunity for carrying out multiobjective optimization. In the industrial reactor, the vapor release rate *history*, $V_T(t)$, and the jacket fluid temperature, T_J (a constant *value*), are used as the control (or optimizing) variables. These two constitute our control vector, $\mathbf{u}$. Thus, our optimization problem can be written in mathematical form, as

$$\underset{T_J, V_T(t)}{\mathrm{Min}} \ \mathbf{I} \equiv [I_1, I_2]^T \tag{a}$$

where

$$I_1^{(i)} = t_f^{(i)}/t_{f,\mathrm{ref}} + w_1(1 - \mu_{n,f}^{(i)}/\mu_{n,\mathrm{ref}})^2 \tag{b}$$

$$I_2^{(i)} = [C_2]_f^{(i)}/[C_2]_{f,\mathrm{ref}} + w_2(1 - \mu_{n,f}^{(i)}/\mu_{n,\mathrm{ref}})^2; \quad i = 1, 2, \ldots, N_P \tag{c}$$

$$\mathrm{conv}_f = \mathrm{conv}_{f,\mathrm{ref}} \tag{d}$$

$$\text{mass and energy balance equations} \tag{e}$$

any additional physical limits

$$\text{on the control variables} \tag{f}$$

(6)

The solution of the multiobjective optimization problem described in eq. (6) is obtained using the nondominated sorting genetic algorithm (NSGA)[22] *adapted in this study* so as to apply for control variables which are continuous functions of time, t. Details of this adapted NSGA are described below, and the associated flowchart is given in Table II. The numbers in the discussion below refer to the numbered boxes in Table II.

Box 4: At generation number, $N_g = 0$, a population having N_P chromosomes (members) is generated. Each chromosome in this population carries the information of one digitized control variable *history* [set of vapor release rate, $V_T(t)/V_{T,\mathrm{max,ref}}$, values] and one control variable *value* (a single value of the jacket fluid temperature, T_J). We discretize our first control variable history, $V_T(t)/V_{T,\mathrm{max,ref}}$, in terms of N_{ga} equispaced points in $0 \le t \le t_{f0}$ (t_{f0}, an initial estimate of t_f, is to be

Table II Flowchart Describing the NSGA[22] as Adapted in This Study

1. Input data:

$$N_P, N_{\text{str}}, N_{\text{ga}}, N_{\text{sim}}, p_m, p_c, q, \alpha,$$
$$t_{f0}, u_{P,k}^{\min}, u_{P,k}^{\max} (k = 1, 2, \ldots, N_{\text{ga}}), T_J^{\min}, T_J^{\max}, N_{\text{g,max}}$$
$$N_{\text{chr}} = (N_{\text{ga}} + 1) \times N_{\text{str}}$$

2. Initialize generation number:

$$N_{\text{g}} = 0$$

3. Initialize random number generator.

4. Create N_P random binary chromosomes, each of length N_{chr} having N_{str} binaries for each of the N_{ga} points representing $u_P(t)$ history and N_{str} binaries (bits) representing the single value of T_J:

$$\mathbf{s}^{(i)} \equiv \left[\mathbf{s}_1^{(i)}, \mathbf{s}_2^{(i)}, \ldots, \mathbf{s}_{N_{\text{ga}}}^{(i)}, \mathbf{s}_{N_{\text{ga}}+1}^{(i)}\right]$$
$$\text{where } \mathbf{s}_k^{(i)} \equiv \left[b_{1,k}^{(i)}, b_{2,k}^{(i)}, \ldots, b_{N_{\text{str}},k}^{(i)}\right]$$

where $b_{j,k}^{(i)} \in \{0, 1\}$

$$i = 1, 2, \ldots, N_P; j = 1, 2, \ldots, N_{\text{str}}; k = 1, 2, \ldots, N_{\text{ga}} + 1$$

5. Decode and adaptively map each chromosome to give a digitized $u_P(t)$ history with N_{ga} real values and a real value of T_J, using

$$u_{P,k}^{(i)} = u_{P,k}^{\min} + \frac{u_{P,k}^{\max} - u_{P,k}^{\min}}{2^{N_{\text{str}}} - 1} \times (\text{decoded value of } \mathbf{s}_k^{(i)})$$
$$T_J^{(i)} = T_J^{\min} + \frac{T_J^{\max} - T_J^{\min}}{2^{N_{\text{str}}} - 1} \times (\text{decoded value of } \mathbf{s}_{N_{\text{ga}}+1}^{(i)})$$
$$k = 1, 2, \ldots, N_{\text{ga}}; i = 1, 2, \ldots, N_P$$

6. For each chromosome, use Hermite interpolation of the N_{ga} discrete values $u_{P,k}^{(i)}$, of $u_P(t)$ to get a continuous $u_P(t)$ history. Obtain N_{sim} ($\gg N_{\text{ga}}$) equispaced intermediate real values, $[U_{P,l}^{(i)}]$; $l = 1, 2, \ldots, N_{\text{sim}}$, describing the $u_P(t)$ history:

$$\left[\mathbf{U}_P^{(i)}\right] = \left[U_{P,1}^{(i)}, U_{P,2}^{(i)}, \ldots, U_{P,N_{\text{sim}}}^{(i)}\right]$$

7. For each chromosome representing a $U_P^{(i)}(t)$ history and a value of $T_J^{(i)}$, solve the model equations [eq. (2)] using Gear's algorithm with stopping condition as $\text{conv}_f = \text{conv}_{f,\text{ref}}$. Record $I_1^{(i)}$ and $I_2^{(i)}$.

   Compute the fitness values, $F_1^{(i)}$ and $F_2^{(i)}$, as $F_m^{(i)} = 1/(1 + I_m^{(i)})$; for all $i = 1, 2, \ldots, N_P$ and $m = 1, 2$. Identify all feasible solutions.

Table II *Continued*

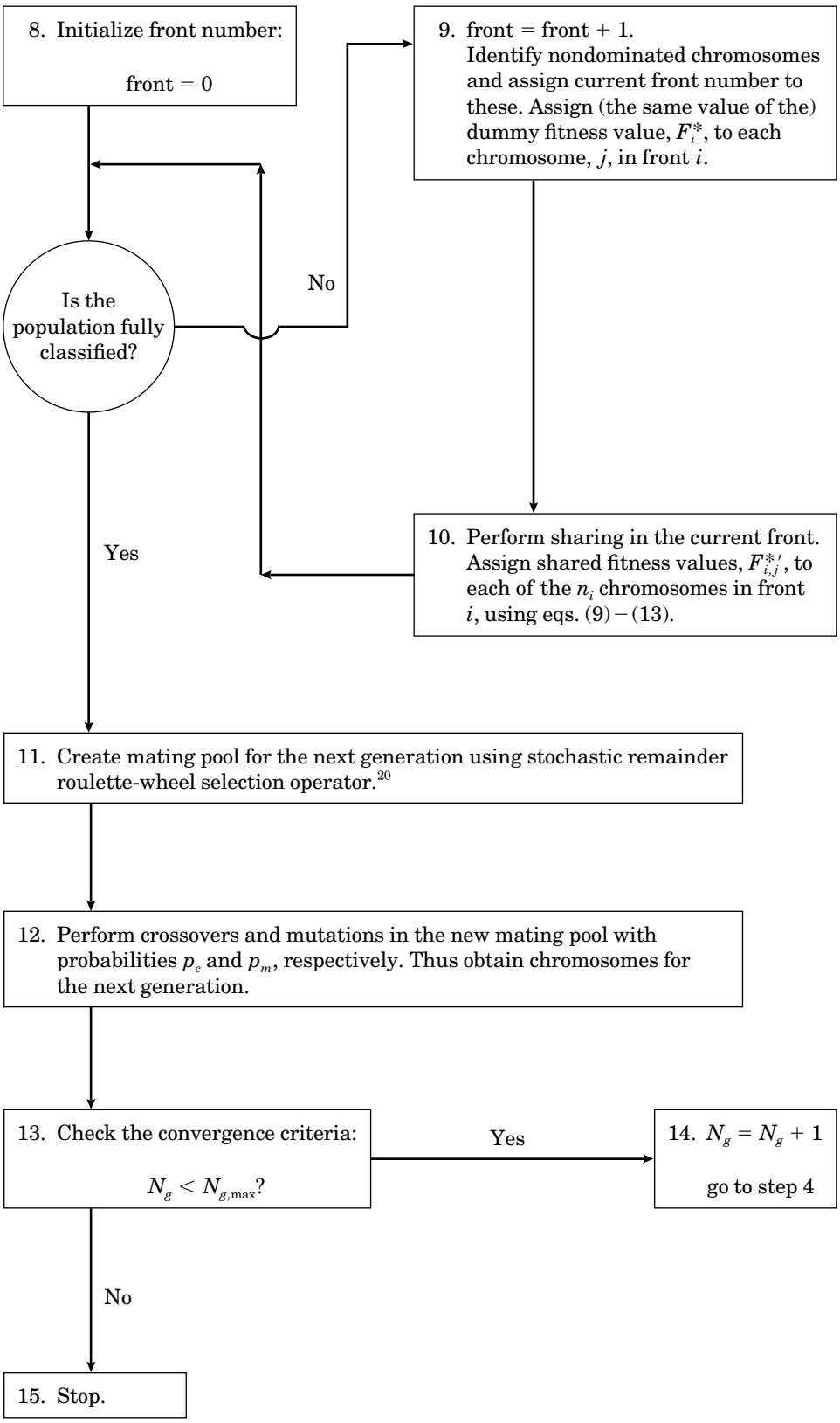

supplied). The second control variable, T_J, is appended in any chromosome as an additional [$(N_{ga} + 1)$th] point. Thus, each of the N_p chromosomes (called strings) comprises a sequence of $(N_{ga} + 1)$ numbers (called substrings). Each of these substrings, in turn, comprises a set of N_{str} binary numbers (0 or 1). Each chromosome, therefore, has $N_{\text{chr}} = (N_{ga} + 1) \times N_{\text{str}}$ binary digits, $b_{j,k}^{(i)}$ (see Box No. 4 of Table II). The N_{chr} individual binaries in each of the N_p chromosomes are generated using a random number generation subroutine.[9,20,21]

Box 5: The complete binary string (sequence of N_{chr} binaries) of the ith chromosome, when decoded into real numbers, $u_{P,k}^{(i)}$ or $T_J^{(i)}$ and interpolated (mapped) between the upper ($u \leq u^{\max}$) and lower ($u \geq u^{\min}$) bounds of the control variables $\mathbf{u}$, at that location, gives a digitized $u_P^{(i)}$ history (a set of N_{ga} real values), [$u_{P,1}^{(i)}$, $u_{P,2}^{(i)}$, ..., $u_{P,N_{ga}}^{(i)}$], representing a $V_T(t)/V_{T,\max,\text{ref}}$ history as well as a value, $T_J^{(i)}$, representing a single value of the jacket fluid temperature T_J, corresponding to that chromosome. Thus, there is a set of N_P chromosomes, each representing a digitized $u_p(t)$ [$\equiv V_T(t)/V_{T,\max,\text{ref}}$] history and a value of T_J, each appropriately coded, in the form of a string of N_{chr} binaries. The minimum difference between the digitized values of the control variable (at any value, t_k) of two different chromosomes is $(u_{P,k}^{\max} - u_{P,k}^{\min})/(2^{N_{\text{str}}} - 1)$. This is the accuracy to which any particular u_P can be determined for different members of the population in a particular generation.

Box 6: The decoded and adaptively mapped, discretized values, $u_{P,k}^{(i)}$, are curve-fitted piecewise (splines) to obtain a continuous *function,* $U_P^{(i)}(t)$. A piecewise cubic Hermite subroutine (E01BFF from the NAG library) is used to do this. This continuous function is again digitized to give N_{sim} ($\geq N_{ga}$) values of the control variable, [$U_{P,l}^{(i)}$; $l = 1, 2, \ldots, N_{\text{sim}}$].

Box 7: These more closely spaced, discretized values of $U_P^{(i)}(t)$ and the value of $T_J^{(i)}$ are fed to the simulation package, D02EJF (of NAG library), which integrates the state-variable equations [eq. (2)] starting with the given initial conditions[12] and terminating at the stopping condition, $\text{conv}_f = \text{conv}_{f,\text{ref}}$. The simulation program stores the values of each of the state variables, $\mathbf{x}^{(i)}(j)$, at every N_{sim} intermediate values of t, such that there are sets of $\mathbf{x}$ values until $\text{conv}_f = \text{conv}_{f,\text{ref}}$. These detailed histories could be printed out later for the optimal solutions. The values of the two objective functions, $I_1^{(i)}$ and $I_2^{(i)}$ [at the final reaction time $t = t_f$, see eqs. 6(b,c)], are computed. One additional point needs to be emphasized: The computer codes involving GA usually *maximize* a fitness function, $F_m^{(i)}$, rather than minimize objective functions, $I_m^{(i)}$, $m = 1, 2$. Hence, we define fitness functions to convert the minimization problem to an equivalent maximization problem as follows:

$$F_1^{(i)} \equiv 1/(1 + I_1^{(i)})$$
$$F_2^{(i)} \equiv 1/(1 + I_2^{(i)}) \qquad (7)$$

It may be added that the technique described until this stage is quite similar to that[9] developed for the optimization of MMA polymerization. All the feasible points are identified (for plotting) at this stage. The feasible points or chromosomes are those for which $\text{conv}_f = \text{conv}_{f,\text{ref}} \pm 0.009$ and $(1 - \mu_{n,f}/\mu_{n,\text{ref}}) = \pm 0.009$. The satisfaction of the latter requirement means that the penalty values in eqs. (4) and (5) are negligible.

Box 9: A chromosome, i_1, is said to be dominated by another chromosome, i_2 (for the present problem of minimization of $\mathbf{I}$ or maximization of $\mathbf{F}$), if

$$F_1^{(i_1)} < F_1^{(i_2)} \qquad \text{(a)}$$

as well as

$$F_2^{(i_1)} < F_2^{(i_2)} \qquad \text{(b)}$$

then

$$i_1 \text{ is dominated by } i_2 \qquad (8c)$$

For example, in Figure 3, point 3 is dominated by point 5. We test each of the N_P chromosomes in the population against all others to sort out *all* dominated chromosomes. As soon as a chromosome is found to be dominated, it is not checked for dominance with any other chromosome in the population. When all chromosomes have been checked for dominance, and all dominated chromosomes have been identified, the *rest of the chromosomes* are given a front number, FRONT = 1. These chromosomes having FRONT = 1, are called nondominated chromosomes. In Figure 3, points 4, 5, and 6 will constitute the chromosomes assigned FRONT = 1. All nondominated chromosomes are then assigned a *dummy* fitness value, F_1^*, equal to N_P. Thereafter, these *dummy* fitness values are modified according to the *sharing* pro-

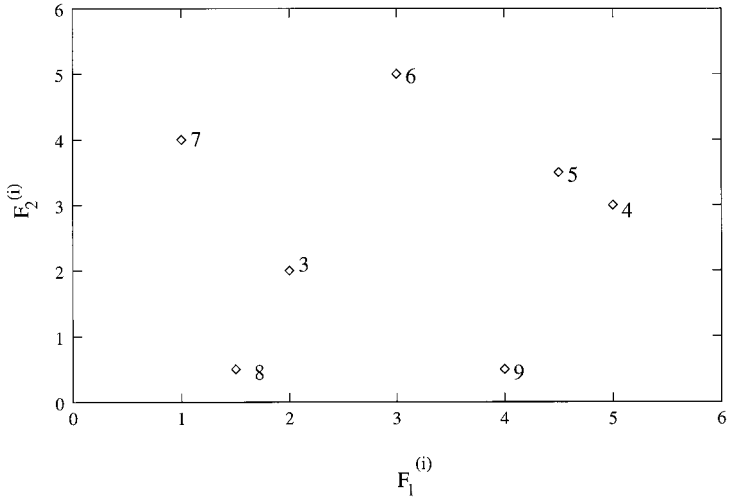

Figure 3 An example describing the concept of dominance.

cedure described in item 10 below, to assign a *shared fitness* value. Sharing is done to maintain diversity in the nondominated chromosomes.[27] To identify chromosomes for other fronts, we temporarily discard all nondominated chromosomes. The *remaining* chromosomes are again checked for dominance using eq. (8) and new nondominated chromosomes are sorted and given a front number, FRONT = 2. Again, the new nondominated chromosomes (in FRONT 2) are given a dummy fitness value, F_2^*, which is slightly smaller than the lowest of the *shared* fitness values of the previous front. The sharing of the dummy fitness values is performed again, and a shared fitness value is assigned to each nondominated chromosome. This procedure is continued until all N_P chromosomes have been given a front number.

Box 10: *Sharing*—Sharing is performed among the members of the ith front (having n_i members) using the following procedure:

(a) For each chromosome, j, in front i, the dimensionless distance, d_{jk}, of this chromosome from any other chromosome, k, (including j) in the (same) front is calculated using

$$d_{jk} = \left\{ \sum_{l=1}^{N_{g\alpha}} [(u_{P,l}^{(j)} - u_{P,l}^{(k)})/(u_{P,l}^{\max} - u_{P,l}^{\min})]^2 + [(T_J^{(j)} - T_J^{(k)})/(T_J^{\max} - T_J^{\min})]^2 \right\}^{1/2} \quad (9)$$

(b) We calculate the *niche count,* m_j, using

$$m_j = \sum_{k=1}^{n_i} Sh(d_{jk}) \quad (10)$$

where

$$Sh(d_{jk}) = \begin{cases} 1 - \left(\dfrac{d_{jk}}{\sigma_{\text{share}}}\right)^{\alpha}, & \text{if } d_{jk} < \sigma_{\text{share}}; \\ 0, & \text{otherwise} \end{cases} \quad (11)$$

σ_{share} is given by

$$\sigma_{\text{share}} = \frac{1}{2q^{[1/(N_{g\alpha}+1)]}}. \quad (12)$$

In eq. (12), q is the number of Pareto optimal points desired (we have used $q = 15$ in our study). The parameter, α, is an exponent which controls the sharing effect (we have used $\alpha = 2$ in the present study).

(c) The dummy fitness, F_i^*, of each chromosome, j, in front, i, is modified by dividing F_i^* by the chromosome's niche count, m_j, to calculate the shared fitness value, $F_{ij}^{*\prime}$, as follows:

$$F_{ij}^{*\prime} = \frac{F_i^*}{m_j} \tag{13}$$

Box 11: The stochastic remainder roulette wheel selection[20] procedure is used on the shared fitness values, and a mating pool of N_P chromosomes is generated. This procedure involves proportionate selection, where, first, the number of copies made of each chromosome is equal to the integer part of the value of $F_{ij}^{*\prime}/\bar{F}_{ij}^{*\prime}$. Here, $\bar{F}_{ij}^{*\prime}$ is the average of the shared fitness values of all the N_P chromosomes in the population. Additional copies of the jth chromosome in the ith front (to make a total of N_P in the mating pool) are made, thereafter, using a roulette wheel with probability proportional to the fractional part of $F_{ij}^{*\prime}/\bar{F}_{ij}^{*\prime}$.

Box 12: After the mating pool is created, crossover and mutation take place to produce the new population (next generation). These operations take place at the chromosome (binary) level. Two chromosomes are randomly selected from the mating pool, a crossing site is selected (randomly again), and portions of the chromosomes before and after the crossing site are exchanged. For example, for seven-bit chromosomes with the crossing site after the third binary, the crossover is described by the following:

$$\begin{array}{cc} 100|1111 & \longrightarrow \quad 100 \quad 0100 \\ 110|0100 & \longrightarrow \quad 110 \quad 1111 \\ \text{(old generation)} & \text{(new generation)} \end{array} \tag{14}$$

While performing crossovers, only $p_c N_P$ chromosomes are crossed, the remaining being left untouched (p_c is referred to as the crossover probability).

Another operation, called mutation, is also used to improve the next generation. The mutation operator changes a binary number from 1 to 0 or vice versa, with a probability, p_m. This operation is carried out for each of the $N_P N_{\text{chr}}$ bits in the population, again using appropriate random numbers. The need for mutation leads to a local search around the current solution and helps maintain the diversity of the population.

This completes one generation of NSGA. These sets of operations are carried out from one generation to the next until the number of generations equals the maximum number specified at the starting of the program as an input parameter.

In a nutshell, the feasible nondominated solutions are emphasized in every generation by the action of the reproduction operator of NSGA. The coexistence of multiple feasible nondominated solutions is ensured by using the sharing technique. Thereafter, crossover and mutation create new and, hopefully, better feasible nondominated solutions. This process continues, and, finally, the best nondominated solutions of a population converge to the true Pareto optimal solutions. Since diversity in the best feasible nondominated solutions is maintained in each generation, the final population is expected to capture a number of different Pareto optimal solutions simultaneously in one run.

RESULTS AND DISCUSSION

Several checks have been made to ensure that the computer code was free of errors. For example, the values of conv, $[C_2]$, μ_n, etc., for any one chromosome were found to be the same as those obtained using our earlier[12] simulation code [with the same $V_T(t)$ and T_J]. Also, Pareto optimal solutions for some simpler problems[22] were obtained using our code, and they were found to be the same as solutions obtained earlier. The CPU time ($[W]_0 = 3.45\%$) for 20 generations was found to be 144 min on a mainframe HP8000S/950 superminicomputer.

The upper and lower limits of each of the N_{ga} control variables (for $[W]_0 = 3.45\%$), $u_{P,k}^{\max}$ and $u_{P,k}^{\min}$, $k = 1, 2, \ldots, N_{ga}$, as well as of the jacket fluid temperature, $T_J^{\max}$ and $T_J^{\min}$, were first determined. It was found that these (slightly restricted) search "windows" for $V_T/V_{T,\max,\text{ref}}$ and T_J were necessary and that very large search domains on these two control variables led to severe computational problems with no Pareto solutions being obtained. Since our earlier multiobjective optimization study[28] of this reactor (with the *shape* of the pressure history fixed and described by four *values* only) gave us an optimal $V_T/V_{T,\max,\text{ref}}$ history and an optimal value of T_J, we selected the windows of these control variables around these previous solutions[28] as

$$0.4 \times (V_T/V_{T,\max,\text{ref}})_{28} \le V_T/V_{T,\max,\text{ref}} \le 1.6 \times (V_T/V_{T,\max,\text{ref}})_{28} \tag{15}$$

Table III Window for $V_T/V_{T,\max,ref}$ Used for Our Study, $[W]_0 = 3.45\%$

k[a]	$(V_T^{opt}/V_{T,\max,ref})_{28}$	$(V_T^{max}/V_{T,\max,ref})$	$(V_T^{min}/V_{T,\max,ref})$
1	0.05	0.3	0.01
2	0.06	0.1	0.02
3	0.2	0.32	0.08
4	0.3	0.48	0.12
5	0.2	0.32	0.08
6	0.07	0.112	0.028
7	0.03	0.048	0.012
8	0.05	0.08	0.02
9	0.02	0.032	0.008
10	0.02	0.032	0.008

[a] $k = 1, 2, \ldots, N_{ga}$.

at corresponding values of t/t_f. The subscript 28 indicates values obtained in ref. 28. The window for T_J was taken as 220°C $\leq T_J \leq$ 270°C. It was found that the window for $V_T/V_{T,\max,ref}$ at $t/t_f = 0$ had to be widened beyond that given in eq. (15) before solutions could be obtained. The exact window used for $V_T/V_{T,\max,ref}$ is given in Table III, while Figure 4 gives the window as well as the optimal values obtained earlier.[28] Any further increase in the width of the window for $V_T/V_{T,\max,ref}$ reduces the number of Pareto points obtained (without any change in the optimal solutions), and no further widening of the width of the window was attempted. The values of the computational parameters used in the optimization study are given in Table IV. The initial and other values associated with the reactor (including "reference" values) are the same as those given in ref. 12.

Figure 5 shows the feasible solutions at the beginning ($N_g = 0$) for $[W]_0 = 3.45\%$. Each of these points satisfies all the constraints of the system [eqs. 6(d)–(f), and $\mu_n = \mu_{n,ref}$ within error bounds]. Convergence to the optimal Pareto set (shown in Fig. 6) is observed to take about eight generations. The number of Pareto points obtained finally (10) is found to be of the same order as q (15), as expected. The solution in Figure 6 is referred to as the "reference" run. The Pareto sets obtained for the other two water concentrations, that is, $[W]_0 = 2.52$ and 4.43%, are given in Figure 7. It may be added that the values of $[C_2]_{f,ref}$ are different for the three cases, while $t_{f,ref}$

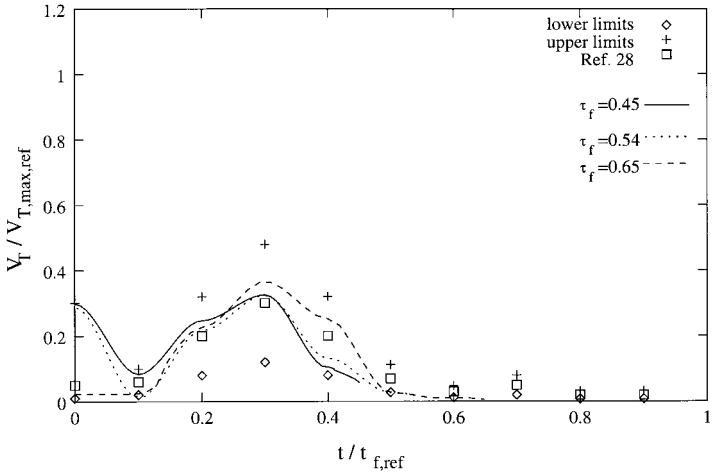

Figure 4 Dimensionless vapor release rate histories for $[W]_0 = 3.45\%$, for three points ($t_f/t_{f,ref} = 0.45, 0.54, 0.65$) on the Pareto optimal set. (◇) Lower and (+) upper limits of the window used in this study; (□) optimal values of $V_T/V_{T,\max,ref}$ as obtained in ref. 28.

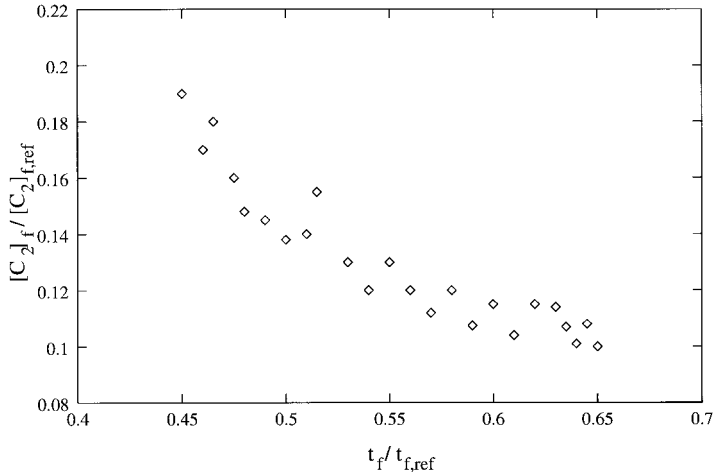

Figure 5 Feasible points at generation number ($= N_g$) = 0, for $[W]_0 = 3.45\%$.

is the same. The values of $u_{P,k}^{\max}$, $u_{P,k}^{\min}$ ($k = 1, 2, \ldots, N_{ga}$), $T_J^{\max}$ and $T_J^{\min}$, as well as all the other computational parameters, for all these three cases are taken to be the same as given in Tables III and IV. It can be observed that any point on the Pareto set is not inferior to any other, because, while going from one point to another, one improves one objective function while worsening the other.

After the generation of the Pareto sets, a designer can choose an operating point (preferred solution) from these sets using his or her intuition [or other information not included in eq. (6)]. One technique which can be used is to select the preferred solution as a point nearest to a point, U_i, called utopia. The point, U_i, is obtained by performing two single-objective function optimizations [i.e., by solving eq. (6) using only one of the two objectives and dropping the other objective function completely]. These two limiting solutions[2,3,28] show up as the straight lines in Figure 6. The intersection of these lines gives the utopia. Point U_i is unattainable, but represents an ideal. The preferred solution is often taken[2,3] to be the point nearest to utopia. This point is denoted by O_i in Figure 6. The subscript, i, on points U_i and O_i corresponds to the integer in the value of the initial water concentration, $[W]_0$. It must be emphasized that the geometrical construction required to obtain points O_i will depend on the

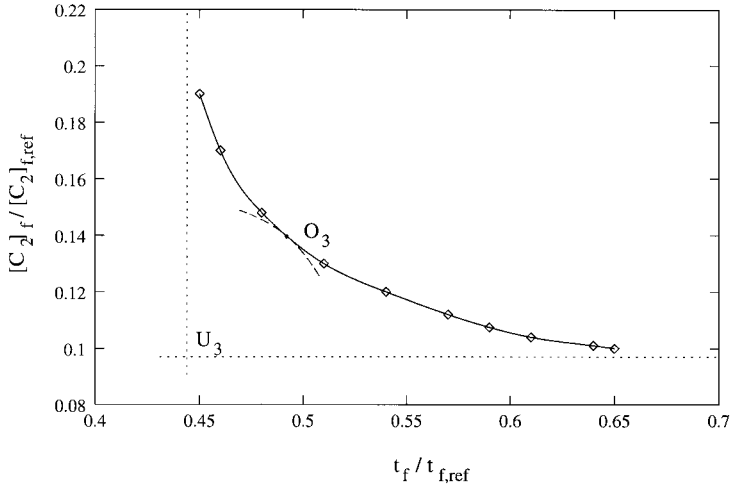

Figure 6 Pareto optimal set (for $N_g = 8$ as well as 20) for $[W]_0 = 3.45\%$. U_3 is the utopia while O_3 is the preferred solution.

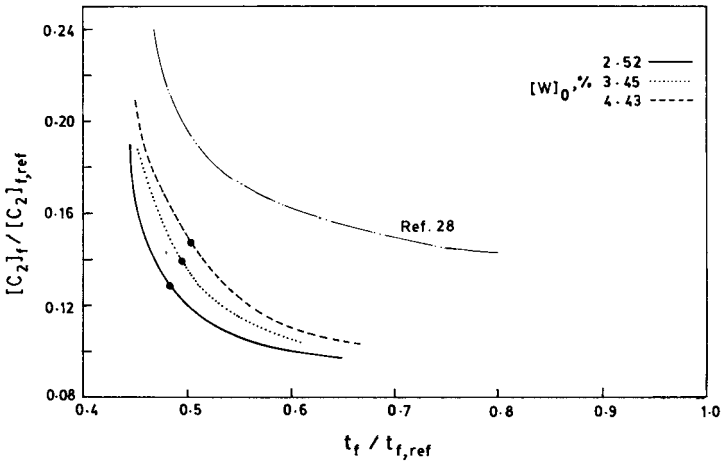

Figure 7 Comparison of the three Paretos (with the preferred solutions indicated by dots) with the Pareto for $[W]_0 = 3.45\%$ obtained by Sareen and Gupta.[28]

scales being used in plotting the Paretos. However, this is the best one can do in absence of additional information.

Each point on the Pareto sets in Figure 7 corresponds to a different $V_T/V_{T,\max,\text{ref}}$ history as well as T_J. Three of these histories (for $t_f/t_{f,\text{ref}} = 0.45$, 0.54, and 0.65 on the Pareto for the reference case of $[W]_0 = 3.45\%$) are shown in Figure 4. Figure 8 shows the optimal values of T_J corresponding to the Paretos for all three values of $[W]_0$.

In Figure 7, the Pareto sets obtained in the present study are compared with the Pareto set obtained by Sareen and Gupta[28] for $[W]_0 = 3.45\%$. The Paretos obtained in the present case indicate superior performance compared to that obtained earlier. This indicates that "freezing" of the *shape* of the pressure history during optimization does not give the best optimal solutions, since the search space becomes limited by this procedure, a drawback that does not exist in the current, more general, study.

Table IV Computational Parameters Used in the Reference Run

$(V_T/V_{T,\max,\text{ref}})_k^{\min,\max}$; $k = 1, 2, \ldots, N_{\text{ga}}$; (as in Table III)
$T_J^{\max} = 270.0°\text{C}$
$T_J^{\min} = 220.0°\text{C}$
$N_{\text{ga}} = 10$
$N_P = 80$
$N_{\text{str}} = 7$
$N_{\text{sim}} = 100$
$q = 15$
$\alpha = 2$
$p_c = 0.99$
$p_m = 0.001$
$N_{\text{g,max}} = 20$
$N_{\text{chr}} = (10 + 1) \times 7 = 77$
$w_1 = w_2 = 0.25 \times 10^6$

Figure 9 shows the optimal history of $V_T/V_{T,\max,\text{ref}}$ for the preferred solution, O_3, and compares it with values currently in use.[12] It is observed that the vapor release rate is finite at the beginning in the case of the optimal solution, in contrast to the present operation. Also, the maximum value of the optimal vapor release rate is lower. It must be ensured that the values of V_T indicated in the beginning can, indeed, be attained (the pressure inside the reactor may not be high enough to provide such release rates even with a fully open control valve). Figure 10 shows that higher vapor release rates are required for higher values of $[W]_0$. Figure 2 shows the variation of the dimensionless pressure, Π, with dimensionless time for the preferred solutions (O_2, O_3, and O_4). Much lower pressures are required as compared to the current operation. Figure 11 shows the variation of the dimensionless temperature with dimensionless time for the three preferred solutions. The temperatures are observed to increase more slowly as compared to current values. This is because of nonzero vapor release rates at the beginning (leading to higher amounts of vaporization). In Figure 12, the number-average chain length, μ_n, versus the dimensionless time, is plotted for the three preferred solutions. The plateau observed currently is found to be missing in the case

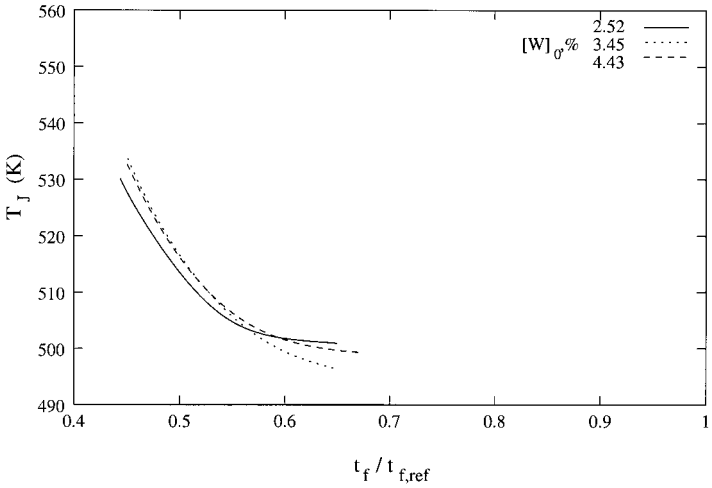

Figure 8 Jacket fluid temperatures corresponding to different points on the three Paretos.

of the optimal runs. This is similar to the observation made by Sareen and Gupta.[28] In Figure 13, the monomer conversion, conv, is plotted against the dimensionless time. The delayed attainment of the equilibrium values is observed. In Figure 14, $[C_2]/[C_2]_{f,\mathrm{ref},3}$ (where subscript 3 indicates that the reference value, $[C_2]_{f,\mathrm{ref}}$, for $[W]_0 = 3.45\%$ is used for all three cases) is plotted against the dimensionless time for the preferred solutions as well as for the current operation. Use of the same denominator for all three $[W]_0$ helps to compare the values of $[C_2]$ better. Our theoretical results indicate that the amount of cyclics expected to be produced under optimal operating conditions is much smaller than that produced currently. This is also indicated in Figure 7. The quality of the product produced under optimal conditions is, thus, observed to be far better (while the total reaction time, t_f, is also substantially reduced leading to higher plant capacities).

The effect of varying the several computational parameters given in Tables III and IV on the Pareto solution for $[W]_0 = 3.45\%$ was then studied. If the population size, N_P, is decreased from the reference value of 80 to 60, the same Pareto is obtained. We could, as well, choose to use $N_P = 60$ since the number of function evaluations would be lower. However, increase in N_P to 100

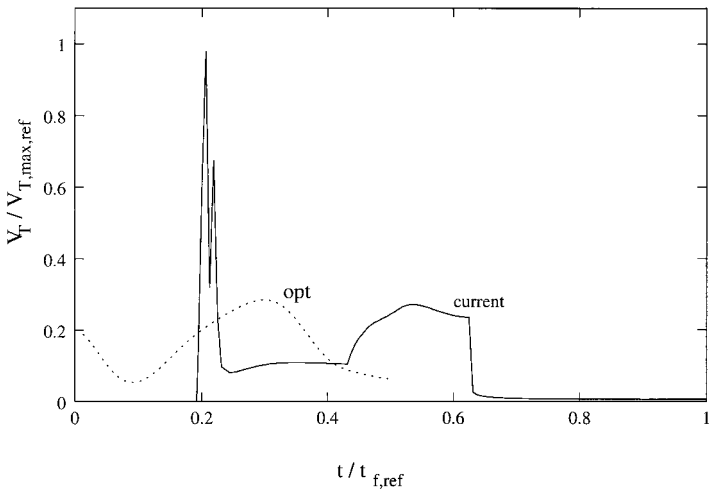

Figure 9 Variation of the dimensionless vapor release rate with dimensionless time for the current and optimal (preferred solution, O_3) cases; $[W]_0 = 3.45\%$.

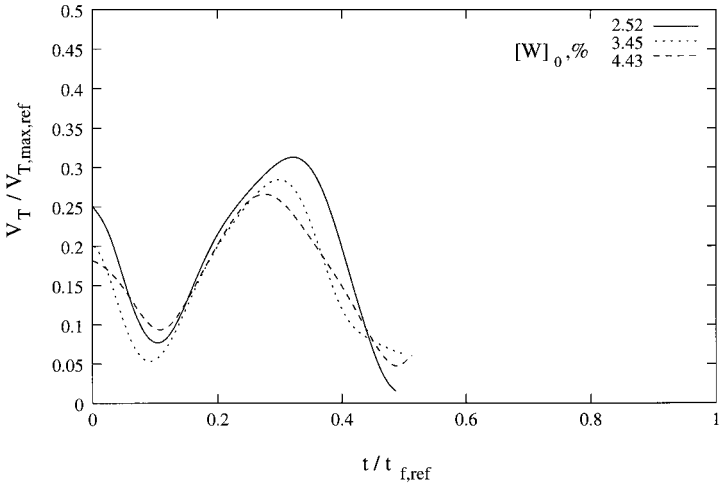

Figure 10 Dimensionless vapor release rate histories for the preferred solutions for $[W]_0$ = 2.52, 3.45, and 4.43%.

led to severe memory and CPU time requirements, and only three generations could be completed. A few extra feasible solutions were found for $N_P = 100$ than shown in Figure 5. The evolving Pareto appeared to be identical. On increasing the value of N_{str} from 7 to 10, we obtained Pareto solutions which differed only in the fifth to seventh decimal places. This increased accuracy is, thus, not necessary and the reference value $N_{str} = 7$ is allright. Similarly, increase in the value of N_{ga} from 10 to 16 led to no significant changes in the Pareto set. The effect of varying the value of the crossover probability, p_c, from 0.99 to 0.77, again, led to no significant changes in the optimal solutions. The effect of a change in the value of the mutation probability, p_m, from 0.001 to 0.1, led to fewer points on the Pareto set (the ones obtained were identical to those in the reference case), but convergence was attained more slowly (at the 18th generation). Also, higher p_m led to some erratic behavior in the feasible points obtained in each generation in the beginning (this was probably the cause of slow convergence). Decrease as well as minor increase of the window provided for $V_T/V_{T,\max,\text{ref}}$ (to factors of 0.2 and 1.2 or 0.7 and 1.7, of the values in ref. 28) led to fewer points on the Pareto (although the same values were obtained for the points). The reference val-

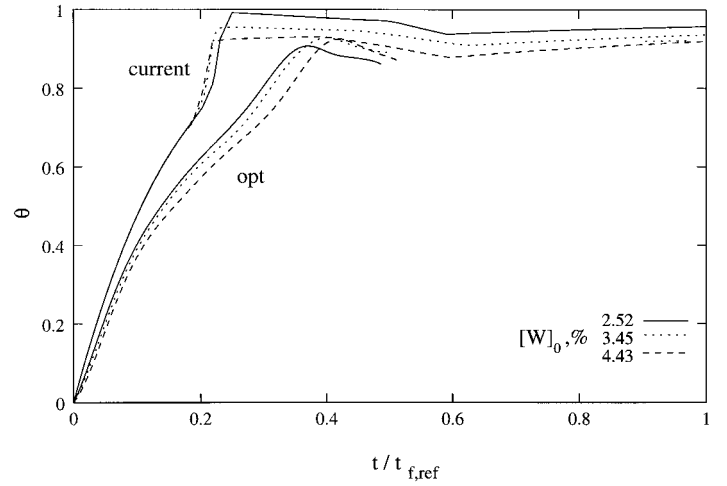

Figure 11 Variation of the dimensionless temperature with dimensionless time for the current and optimal (preferred solutions) cases, for $[W]_0$ = 2.52, 3.45, and 4.43%.

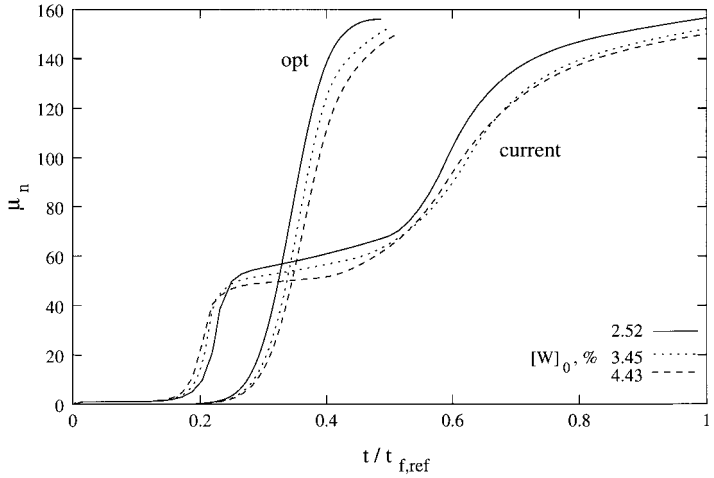

Figure 12 Variation of the degree of polymerization with dimensionless time for the current and optimal (preferred solutions) cases, for $[W]_0$ = 2.52, 3.45, and 4.43%.

ues of the computational parameters in Tables III and IV, thus, appear justified.

CONCLUSIONS

Pareto optimal solutions have been obtained for the multiobjective optimization problem described in eq. (6). The vapor release rate *history,* $V_T(t)$, and the value of the jacket fluid temperature, T_J, have been used as the control (optimizing) variables. An adapted nondominated sorting genetic algorithm (NSGA) technique was used to obtain the solutions. Use of this niche-based search technique was found to be superior to the use of Pontryagin's minimum principle for dynamic optimization.[29] In fact, our attempt to extend our earlier work[29] using Pontryagin's principle (for single-objective optimization of the semibatch nylon 6 reactor) to the more difficult problem described in eq. (6) failed due to severe numerical problems. This indicates the superiority of the present technique. It is found that there is considerable scope for improvement in the operation of the industrial reactor (reduced total reaction times, reduced cyclic formation, while simultaneously maintaining

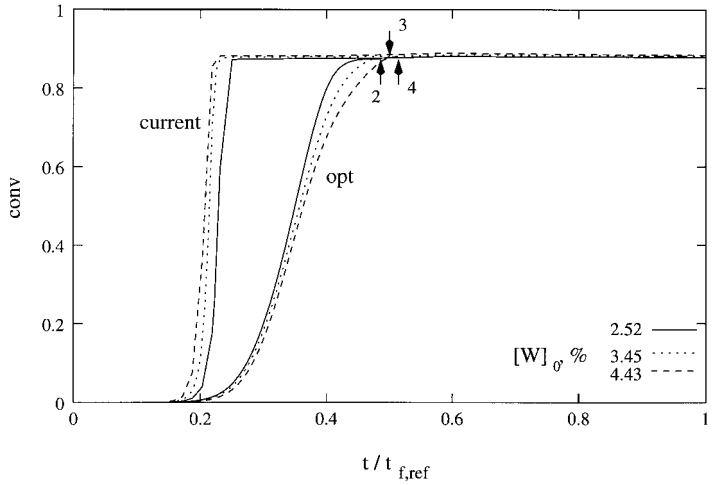

Figure 13 Variation of the monomer conversion with dimensionless time for the current and optimal cases (preferred solutions), for $[W]_0$ = 2.52, 3.45, and 4.43%. Notation for the arrows same as in Figure 2.

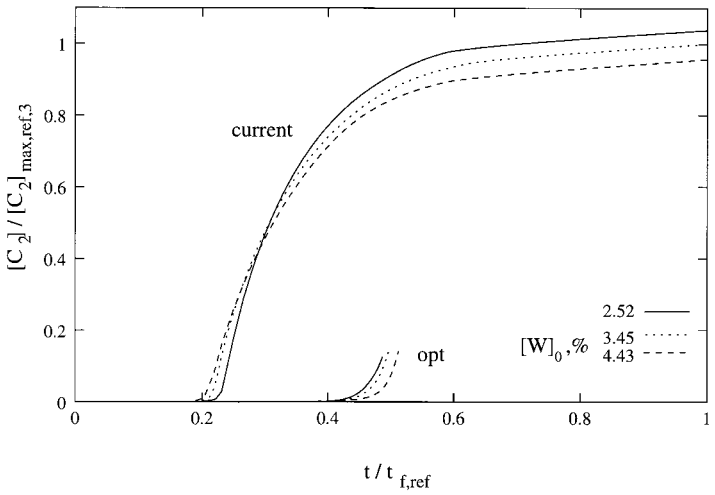

Figure 14 Variation of the dimensionless dimer concentration (using $[C_2]_{f,\text{ref}}$ for $[W]_0 = 3.45\%$ as the normalizing parameter for all three cases) with dimensionless time for the current and optimal cases (preferred solutions), for $[W]_0 = 2.52$, 3.45, and 4.43%.

the values of monomer conversion and the number-average molecular weight). We understand that some improvements (in terms of reduction in the reaction time, t_f) have already been implemented on the industrial reactor recently, along the lines indicated in the present work.

This work was partly funded by a grant from the Research Centre, Gujarat State Fertilizers Co. Ltd., Vadodara, India.

NOMENCLATURE

A_i^0, A_i^c	frequency factor for ith reaction in absence (0) and in presence (c) of catalytic effect (kg mol^{-1} h^{-1} or kg^2 mol^{-2} h^{-1})
conv	monomer conversion [eq. (3)]
C_i	caprolactam ($i = 1$) and cyclic dimer ($i = 2$)
d_{jk}	normalized distance in x space between jth and kth points [eq. (9)]
DP	degree of polymerization of polymer product ($=\mu_n$)
E_i^0, E_i^c	activation energies for the ith reaction in absence (0) and in presence (c) of catalytic effect (J/mol)
$F_m^{(i)}$	fitness function of ith string
F_i^*	dummy fitness value of chromosomes in ith front
$F_{ij}^{*\prime}$	shared fitness value of jth chromosome in ith front
$\bar{F}_{ij}^{*\prime}$	average of the shared fitness values of all the chromosomes in the population
F	mass of liquid in reactor at time t (kg)
ΔH_i	enthalpy of ith reaction (J/mol)
I	vector of objective functions, I_m; $m = 1, 2$
k_i	forward rate constant of ith reaction
k_i'	reverse rate constant of ith reaction
K_i	equilibrium constant for ith reaction
m_j	niche count for jth point in any front
M_n	number-average molecular weight
M_w	weight-average molecular weight
n_i	number of chromosomes in ith front
N_{chr}	total number of binary digits in chromosome $= (N_{ga} + 1) \times N_{\text{str}}$
N_g	generation number
N_{ga}	number of u_P values which GA generates
N_P	number of chromosomes in the population
N_{sim}	number of u_P values after interpolation
N_{str}	number of binary digits representing each of the control variables
O_i	preferred solutions for ith case ($i = 2$, 3, 4 indicating $[W]_0 = 2.52$, 3.45, and 4.43%)

p	pressure (kPa or atm)
p_c	crossover probability
p_m	mutation probability
q	desired number (approximately) of Pareto points required to be generated
R	gas constant (J mol^{-1} K^{-1})
$R_{v,m}$, $R_{v,w}$	rate of vaporization of monomer and water at time t (mol/h)
$\mathbf{s}_k^{(i)}$	substring of N_{str} binary numbers indicating either the value of $u_{P,k}^{(i)}$ or $T_J^{(i)}$
Sh	sharing function [eq. (11)]
ΔS_i	entropy change for the ith reaction (J mol^{-1} K^{-1})
S_n	linear n-mer
t	time (h)
t_{f0}	initially assumed value for t_f (h)
t_f	total reaction time (h)
T	temperature (K)
T_J	jacket fluid temperature (K)
TOL	tolerance in D02EJF code of NAG library
$T_J^{\min}$, $T_J^{\max}$	lower and upper bounds on jacket fluid temperature
$\mathbf{u}$	vector of control variables, [$u_P(t)$, T_J]
$u_{P,k}^{(i)}$	value of control variable $(V_T/V_{T,\max,\text{ref}})_k^{(i)}$ at the end of kth time interval in the ith chromosome
$u_{P,k}^{\min}$, $u_{P,k}^{\max}$	lower and upper bounds on control variable at the end of kth time interval
U_i	utopia for ith case (i = 2, 3, 4 indicating $[W]_0$ = 2.52, 3.45, and 4.43%)
V_T	rate of vapor release from reactor (mol/h)
w_1, w_2	weightage factors
W	water
$\mathbf{x}$	vector of state variables, x_i

Greek Letters

α	exponent controlling the sharing effect
ζ_i	total mol of m (i = 1), w (i = 2) or both (i = 3) vaporized until time t (mol)
θ	dimensionless temperature
μ_k	kth moment of the chain-length distribution (k = 0, 1, 2, . . . ,); $\mu_k \equiv \sum_{n=1}^{\infty} n^k[S_n]$ (mol/kg)
μ_n	number-average chain length ($\equiv \mu_1/\mu_0$)
Π	dimensionless pressure [eq. 1(a)]
τ	dimensionless time [eq. 1(b)]
σ_{share}	maximum normalized distance in x space between any two points [eq. (12)]

Subscripts/Superscripts

d	desired value
f	final (value for the product)
J	jacket
m	monomer
max	maximum value
0	feed conditions
ref	reference (value used in industrial reactor currently)
t_f	value at $t = t_f$
w	water

Symbols

[ ]	concentrations (mol/kg mixture)

REFERENCES

1. J. N. Farber, in *Handbook of Polymer Science and Technology,* Vol. 1, N. P. Cheremisinoff, Ed., Marcel Dekker, New York, 1989, p. 429.
2. Y. Y. Haimes, *Heirarchial Analysis of Water Resources Systems,* McGraw-Hill, New York, 1977.
3. V. Chankong and Y. Y. Haimes, *Multiobjective Decision Making—Theory and Methodology,* Elsevier, New York, 1983.
4. R. M. Wajge and S. K. Gupta, *Polym. Eng. Sci.,* **34,** 1161 (1994).
5. A. Tsoukas, M. Tirrel, and G. Stephanopoulos, *Chem. Eng. Sci.,* **37,** 1785 (1982).
6. L. T. Fan, C. S. Landis, and S. A. Patel, in *Frontiers in Chemical Reaction Engineering,* L. K. Doraiswamy and R. A. Mashelkar, Eds., Wiley Eastern, New Delhi, 1984, p. 609.
7. J. N. Farber, *Polym. Eng. Sci.,* **34,** 1161 (1994).
8. D. Butala, K. Y. Choi, and M. K. H. Fan, *Comput. Chem. Eng.,* **12,** 1115 (1988).
9. S. S. S. Chakravarthy, D. N. Saraf, and S. K. Gupta, *J. Appl. Polym. Sci.,* **63,** 529 (1997).
10. A. Gupta, S. K. Gupta, K. S. Gandhi, M. H. Mehta, M. R. Padh, A. V. Soni, and B. V. Ankleswaria, *Chem. Eng. Commun.,* **113,** 63 (1992).
11. A. Gupta, S. K. Gupta, K. S. Gandhi, M. H. Mehta, M. R. Padh, A. V. Soni, and B. V. Ankleswaria, in

Recent Trends in Chemical Reaction Engineering, B. D. Kulkarni, R. A. Mashelkar, and M. M. Sharma, Eds., Wiley Eastern, New Delhi, 1987, p. 281.
12. R. M. Wajge, S. S. Rao, and S. K. Gupta, *Polymer,* **35,** 3722 (1994).
13. W. H. Ray and J. Szekely, *Process Optimization,* Wiley, New York, 1969.
14. L. Lapidus and R. Luss, *Optimal Control of Engineering Processes,* Blaisdell, Waltham, MA, 1967.
15. N. R. Vaid and S. K. Gupta, *Polym. Eng. Sci.,* **31,** 1708 (1991).
16. A. K. Ray and S. K. Gupta, *J. Appl. Polym. Sci.,* **30,** 4529 (1985).
17. A. K. Ray and S. K. Gupta, *Polym. Eng. Sci.,* **26,** 1033 (1986).
18. D. Srivastava and S. K. Gupta, *Polym. Eng. Sci.,* **31,** 596 (1991).
19. J. H. Holland, *Adaptation in Natural and Artificial Systems,* University of Michigan Press, Ann Arbor, MI, 1975.
20. D. E. Goldberg, *Genetic Algorithms in Search, Optimization and Machine Learning,* Addison-Wesley, Reading, MA, 1989.
21. K. Deb, *Optimization for Engineering Design: Algorithms and Examples,* Prentice-Hall of India, New Delhi, 1995.
22. N. Srinivas and K. Deb, *Evol. Comput.,* **2,** 3 (1995).
23. H. K. Reimschuessel, *J. Polym. Sci. Macromol. Rev.,* **12,** 65 (1977).
24. K. Tai and T. Tagawa, *Ind. Eng. Chem. Prod. Res. Dev.,* **22,** 192 (1983).
25. A. Kumar and S. K. Gupta, *J. Macromol. Sci. Rev. Macromol. Chem. Phys. C,* **26,** 183 (1986).
26. S. K. Gupta, *Numerical Methods for Engineers,* New Age International/Wiley Eastern, New Delhi, 1995.
27. K. Deb, *Genetic Algorithms in Multimodal Function Optimization,* M.S. Thesis, University of Alabama (TCGA Report No. 89002); The Clearinghouse for Genetic Algorithms, University of Alabama, Tuscaloosa, 1989.
28. R. Sareen and S. K. Gupta, *J. Appl. Polym. Sci.,* **58,** 2357 (1995).
29. R. Sareen, N. K. Kohli, and S. K. Gupta, *J. Appl. Polym. Sci.,* **62,** 1219 (1996).